NASA TECHNICAL NOTE

NASA TN D-7676

NASA TN D-7676

COMBINED QUADRUPOLE-DIPOLE MODEL FOR INLET FLOW DISTORTION NOISE FROM A SUBSONIC FAN

by Marvin E. Goldstein, James H. Dittmar, and Thomas F. Gelder

Lewis Research Center
Cleveland, Ohio 44135

NATIONAL AERONAUTICS AND SPACE ADMINISTRATION • WASHINGTON, D. C. • MAY 1974

1. Report No.	2. Government Accession No.	3. Recipient's Catalog No.
NASA TN D-7676		

4. Title and Subtitle	5. Report Date
COMBINED QUADRUPOLE-DIPOLE MODEL FOR INLET FLOW DISTORTION NOISE FROM A SUBSONIC FAN	MAY 1974
	6. Performing Organization Code
7. Author(s)	8. Performing Organization Report No.
Marvin E. Goldstein, James H. Dittmar, and Thomas F. Gelder	E-7881
	10. Work Unit No. 501-04
9. Performing Organization Name and Address	11. Contract or Grant No.
Lewis Research Center National Aeronautics and Space Administration Cleveland, Ohio 44135	
	13. Type of Report and Period Covered
12. Sponsoring Agency Name and Address	Technical Note
National Aeronautics and Space Administration Washington, D.C. 20546	14. Sponsoring Agency Code

15. Supplementary Notes

16. Abstract

A combined quadrupole-dipole model has been developed for the noise generated by inlet flow distortion in a subsonic fan. A formula is derived for the total upstream-radiated acoustic power in each tone as a function of the design parameters of the fan and the properties of the inlet flow distortion. Numerical results are obtained for values of the parameters corresponding to various quiet fans tested at the Lewis Research Center. The analysis is compared with noise measurements taken on a 51-cm (20-in.) diameter research fan as well as with those taken on a number of full-scale fan stages. Fairly good agreement was obtained. It should therefore be possible to use this model to study the noise-reduction potential of the various fan design parameters.

17. Key Words (Suggested by Author(s))	18. Distribution Statement
Fan noise Acoustics Aerodynamic sound	Unclassified - unlimited Category 01

19. Security Classif. (of this report)	20. Security Classif. (of this page)	21. No. of Pages	22. Price*
Unclassified	Unclassified	46	$3.25

* For sale by the National Technical Information Service, Springfield, Virginia 22151

COMBINED QUADRUPOLE-DIPOLE MODEL FOR INLET FLOW DISTORTION NOISE FROM A SUBSONIC FAN

by Marvin E. Goldstein, James H. Dittmar, and Thomas F. Gelder

Lewis Research Center

SUMMARY

A combined quadrupole-dipole model has been developed for the noise generated by inlet flow distortion in a subsonic fan. A formula is derived for the total upstream-radiated acoustic power in each tone as a function of the design parameters of the fan and the properties of the inlet flow distortion. Numerical results are obtained for values of the parameters corresponding to various quiet fans tested at the Lewis Research Center. The analysis is compared with noise measurements taken on a 51-centimeter (20-in.) diameter research fan as well as with those taken on a number of full-scale fan stages. Fairly good agreement was obtained. It should therefore be possible to use this model to study the noise-reduction potential of the various fan design parameters.

INTRODUCTION

The noise generated by single-stage subsonic fans consists of a number of discrete tones, predominantly at the blade passing frequency (BPF), superimposed on a broadband spectrum (which is distributed over a wide range of frequencies). The broadband noise is probably generated by such factors as interaction of the blades with patches of inlet turbulence and irregular vortex shedding by the fan blades. The discrete tones are believed to be caused by periodic spatial nonuniformities (stationary flow distortions) entering the fan and by the passage of its wakes across the stator. However, if the blade passing frequency is large compared with a characteristic turbulence frequency, the sound generated by the inlet turbulence interaction will be concentrated around the harmonics of the blade passing frequency and the spectrum will appear to contain tones of finite width (refs. 1 and 2). Thus, the inlet turbulence interaction may also be a source of pure tones.

On the other hand, it is possible to adjust the ratio of the number of rotor blades to the number of stator blades so that the fundamental blade passing frequency tone generated by the wake interaction mechanism will not propagate (ref. 3). Many single-stage fans have been designed to take advantage of this theoretically predicted "cutoff." However, the results have been disappointing since these fans still exhibit significant fundamental blade passing frequency tones.

A possible explanation for this apparent disagreement with theory is that the tone is being generated by periodic spatial nonuniformities entering the fan. Inlet flow distortion can result from crossflows, wakes from upstream bends or obstructions in or ahead of the duct inlet, and streamwise vortices from nearby surfaces which are sucked into the fan.

When a narrow-band filter is centered (ref. 4) around a BPF tone produced by a fan with no rotor-stator interaction, there are significant amplitude and phase fluctuations in the output. This fluttery signal is quite different from the steady and piercing tone produced by a rotor-stator interaction. It has been argued by Mani (ref. 1) that the "flutteriness" suggests that the tone is produced by inlet turbulence. However, the flutteriness in the tone could just as well be produced by an unsteady inlet flow distortion.

It is shown in reference 2 that the tones produced by inlet turbulence will be much broader than the experimentally observed tones unless the turbulent eddies are extremely large. It would be helpful to measure the frequency of the unsteady flow distortion and compare it with the observed width of the BPF tones.

Additional evidence against turbulence being the source of pure tones is suggested by experiments in which the casing boundary layer (wherein the inlet turbulence entering the fan is most intense) was removed (ref. 5). These experiments indicate a much larger effect of the turbulence on the broadband spectrum than on the pure tone.

The nonuniform flow entering the fan can produce noise through either a quadrupole interaction or a dipole interaction. The quadrupole mechanism is the result of the fluctuating Reynolds stresses in the volume exterior to the blades produced by the interaction of the nonuniform inflow with the potential-flow field of the rotor. The dipole noise is the result of the fluctuating lift on the fan blades resulting from fluctuations in the angle of attack caused by the passage of the blades through the nonuniform flow.

Until fairly recently, all analyses of fan noise considered only the dipole mechanism - the argument that the quadrupoles are less efficient emitters than the dipoles usually being invoked. However, such arguments are valid only when the tip Mach number is small, and "how small" cannot be determined until after the analysis has been made.

The analysis of the flow distortion noise generated through the dipole mechanism is similar to the analysis of the interaction of a rotor with the wakes of an upstream stator. This problem has been studied by a number of investigators (see e.g., refs. 3, 6, and 7). The possibility that inlet flow distortion noise could be generated by a quadrupole

mechanism was first pointed out by Ffowcs-Williams and Hawkings (ref. 8). Morfey (ref. 9) carried out an analysis which indicated that the quadrupole noise could dominate over the dipole noise at Mach numbers as low as 1/2.

In this report, a combined quadrupole-dipole model is developed for predicting inlet flow distortion noise in a high-subsonic-speed fan. The model accounts not only for the individual sources but also for their mutual interactions (which could actually result in cancellation). It is believed that this is the first combined model that has been developed which accounts for the interaction between these two mechanisms. The quadrupole part of the model is a generalization of the one given by Morfey (ref. 9) to include the effects of higher order modes (both radial and circumferential). A much more detailed model of the source is also given. Thus, in the present analysis, all components of the quadrupole which contribute to the sound field are included. The rotor potential-flow field is replaced by a line of discrete vortices.

The analysis leads to a formula for the power emitted from the front of the fan in each tone as a function of the design parameters of the fan and the properties of the inlet flow distortion. Numerical results have been calculated for a range of parameters corresponding to the various quiet fans tested at the Lewis Research Center. The results are compared with experimentally measured tones both from a model fan rotor tested in an indoor compressor aerodynamic performance rig and from full-scale fan stages tested on an outdoor rig.

ANALYSIS

Basic Equations of Sound Emission for Fan Stage

It is shown in section 4.3.1 of reference 10 that the density fluctuation $\rho'(\vec{x}, t)$ at the point $\vec{x}$ and the time t due to the sound emission from a fan in a duct containing a uniform axial flow (with velocity U) is governed by the equation

$$\rho'(\vec{x}, t) = \frac{1}{c_0^2} \int_{-T}^{T} \int_{\nu(\tau)} \frac{\partial^2 G}{\partial y_i \, \partial y_j} T_{ij}^{\dagger} \, d\vec{y} \, d\tau + \frac{1}{c_0^2} \int_{-T}^{T} \int_{S_f(\tau)} \frac{\partial G}{\partial y_j} f_j \, dS(\vec{y}) \, d\tau \qquad (1)$$

where T is some large time interval (which will eventually be put equal to ∞), c_0 is the speed of sound, τ is the time (associated with the source), and f_j is the force exerted on the fluid by the solid boundaries. The function

$$T_{ij}^{\dagger}(\vec{y}, \tau) = \rho v_i^{\dagger} v_j^{\dagger} + \delta_{ij}(p' - c_0^2 \rho') - e_{ij} \tag{2}$$

is Lighthill's stress tensor based on the relative velocity

$$v_i^{\dagger} = v_i - U\delta_{1i} \tag{3}$$

instead of the actual velocity v_i. In this expression p' is the pressure (measured above the ambient pressure p_0), and e_{ij} is the viscous stress tensor. In equation (3) it is assumed that the mean flow is in the x_1-direction. The surface $S_f(\tau)$ over which the second integral is carried out is the surface of the fan blades, and the volume $v(\tau)$ over which the first integral is carried out is the entire region of the duct external to the blades.

The uniformly moving medium, outgoing-wave Green's function G is given by[1]

$$G(\vec{y}, \tau | \vec{x}, t) = \frac{i}{4\pi} \sum_{m,n} \frac{\Phi_{m,n}(y_2, y_3)\overline{\Phi_{m,n}(x_2, x_3)}}{\Gamma_{m,n}} \times \int_{-\infty}^{\infty} \frac{\exp\left\{i\left[\omega(\tau - t) + \frac{Mk}{\beta^2}(y_1 - x_1) + \frac{k_{m,n}}{\beta^2}|y_1 - x_1|\right]\right\}}{k_{m,n}} d\omega \tag{4}$$

where $k = \omega/c_0$, $M = U/c_0$, $\beta = \sqrt{1 - M^2}$, and $\Phi_{m,n}$ denotes a doubly infinite set of eigenfunctions with eigenvalues $\kappa_{m,n}$ determined by solving the Helmholtz equation

$$\left(\frac{\partial^2}{\partial y_2^2} + \frac{\partial^2}{\partial y_3^2}\right)\Phi_{m,n} + \kappa_{m,n}^2 \Phi_{m,n} = 0 \tag{5}$$

on the cross-sectional area A of the duct subject to appropriate homogeneous boundary conditions on the duct surface. Thus, when the surface of the duct is rigid, we must require that

---

[1] The overbar denotes the complex conjugate.

$$\frac{\partial \Phi_{m,n}}{\partial n} = 0 \qquad \text{on surface } S \tag{6}$$

where $\partial/\partial n$ denotes the normal derivative to the duct surface S. The remaining quantities in equation (4) are

$$\Gamma_{m,n} = \int_A |\Phi_{m,n}|^2 \, dy_2 \, dy_3 \tag{7}$$

and

$$k_{m,n} = \sqrt{k^2 - \beta^2 \kappa_{m,n}^2}$$

where, in order to ensure that G represents the outgoing-wave Green's function, we must choose the branch cut of the square root to be as shown in figure 1.

When the observation point is far enough from the source (i.e., in the acoustic regime), the pressure and density fluctuations will be small and we can use the linear approximation

$$p' = c_0^2 \rho' \tag{8}$$

The first term in equation (1) is a volume quadrupole source adjusted to account for reflections at the duct wall. The second term is the usual dipole source for fan noise.

Rectangular Duct Model

In order to model a real fan, the most appropriate cross-sectional shape of the duct is an annulus, such as that shown in figure 2(a). The eigenfunctions $\Phi_{m,n}$ will then be combinations of Bessel functions. The analysis can be considerably simplified, however, by assuming that the duct is "unrolled" into the rectangular strip shown in figure 2(b). (The larger the number of blades, the more closely the rotor approximates a two-dimensional disturbance pattern with subsonic phase speed.) The width δ of the rectangular duct is equal to 2π times the mean radius $\overline{R}$ of the annular duct, and its height b is equal to the outer radius minus the inner radius of the annular duct. In this case, we must require that $\Phi_{m,n}$ and its normal derivative take on the same values on the surface S_a as they do at the corresponding points on the surface S_b (periodicity

condition). It can be verified by substitution that the eigenfunctions of equation (5) which satisfy this condition together with the boundary condition (6) on the upper and lower walls are given by

$$\Phi_{m,n} = e^{i2\pi m y_2/\delta} \cos\left(\frac{n\pi y_3}{b}\right) \quad \text{for} \begin{cases} n = 0, 1, 2, \ldots \\ m = 0, \pm 1, \pm 2, \ldots \end{cases}$$

where the $\vec{y}$-coordinate system is shown in figure 3 and the corresponding eigenvalues are given by

$$\kappa^2_{m,n} = \left[\left(\frac{2m}{\delta}\right)^2 + \left(\frac{n}{b}\right)^2\right]\pi^2 \tag{9}$$

Hence,

$$k_{m,n}(k) = \sqrt{k^2 - \beta^2\pi^2\left[\left(\frac{2m}{\delta}\right)^2 + \left(\frac{n}{b}\right)^2\right]} \tag{10}$$

$$\Gamma_{m,n} = \int_0^{\delta}\int_0^{b} \cos^2\left(\frac{n\pi y_3}{b}\right) dy_2\, dy_3 = \frac{\delta b}{2}\left(1 + \delta_{n,0}\right)$$

and

$$G(\vec{y}, \tau|\vec{x}, t) = \frac{i}{2\pi\delta b} \sum_{m=-\infty}^{\infty} \sum_{n=0}^{\infty} \frac{\cos\left(\frac{n\pi y_3}{b}\right)\cos\left(\frac{n\pi x_3}{b}\right)}{1 + \delta_{n,0}} e^{i\left[2\pi(y_2 - x_2)/\delta\right]m}$$

$$\times \int_{-\infty}^{\infty} \frac{\exp\left\{-i\left[\omega(t - \tau) - \frac{1}{\beta^2}(Mk \pm k_{m,n})(y_1 - x_1)\right]\right\}}{k_{m,n}} d\omega \tag{11}$$

where the upper sign in the exponent corresponds to upstream propagation ($x_1 < y_1$) and the lower sign corresponds to downstream propagation ($x_1 > y_1$).

Transformation to Rotor Coordinates

In order to make the limits of integration in equation (1) independent of time, we introduce the $\vec{\eta}$ coordinate system by

$$\eta_i = y_i + \delta_{i2} U_t \tau \tag{12}$$

where U_t denotes the velocity of the blade row and is taken as positive in the direction shown in figure 3. But since for each value of (y_1, y_2), f_j and $T_{ij}^{\dagger}$ take on the same values at $y_2 = -\delta/2$ as they do at $y_2 = +\delta/2$, they can be extended to continuous periodic functions from $-\infty$ to $+\infty$. And since the Green's function is also periodic, the integration with respect to η_2 can be translated by an arbitrary amount. Thus, the integration in the first integral of equation (1) can be carried out over any region ν_0 (of fixed shape which coincides with $\nu(\tau)$ at some definite instant of time, and the second integral can be carried out over the surface S_f^0 of a fixed set of blades. Equation (1) then becomes

$$p'(\vec{x}, t) = \int_{-T}^{T} \int_{\nu_0} \frac{\partial^2 G}{\partial \eta_i \, \partial \eta_j} T_{ij}^{\dagger}(\vec{\eta}, \tau) \, d\vec{\eta} \, d\tau + \int_{-T}^{T} \int_{S_f^0} \frac{\partial G}{\partial \eta_j} f_j(\vec{\eta}, \tau) \, dS(\vec{\eta}) \, d\tau \tag{13}$$

where the linear approximation (8) has been used.

Derivation of Spectral Equations

Rather than deal with the pressure directly, it is convenient to deal with its spectrum $P(\omega)$ defined by the generalized Fourier transform

$$p' = \int_{-\infty}^{\infty} P(\omega) e^{-i\omega t} \, d\omega \tag{14}$$

It therefore follows upon inserting equation (12) into (11) and using the result in equation (13) that

$$P(\omega) = P_Q(\omega) + P_D(\omega) \tag{14a}$$

where

$$P_Q(\omega) = \sum_{m=-\infty}^{\infty} \sum_{n=0}^{\infty} Q^{\pm}_{m,n}(\omega) C^{\pm}_{m,n}(\vec{x}, \omega) \tag{15a}$$

$$P_D(\omega) = \sum_{m=-\infty}^{\infty} \sum_{n=0}^{\infty} D^{\pm}_{m,n}(\omega) C^{\pm}_{m,n}(\vec{x}, \omega) \tag{15b}$$

$$Q^{\pm}_{m,n}(\omega) = \int_{\nu_0} \left[\frac{\partial^2}{\partial \eta_i \, \partial \eta_j} e^{i(\alpha_1^{\pm}\eta_1 + \alpha_2^{\pm}\eta_2)} \cos(\alpha_3^{\pm}\eta_3) \right] \int_{-T}^{T} e^{i(\omega - 2m\pi U_t/\delta)\tau} T^{\dagger}_{ij} \, d\tau \, d\vec{\eta} \tag{16a}$$

$$D^{\pm}_{m,n}(\omega) = \int_{S_f^0} \left[\frac{\partial}{\partial \eta_j} e^{i(\alpha_1^{\pm}\eta_1 + \alpha_2^{\pm}\eta_2)} \cos(\alpha_3^{\pm}\eta_3) \right] \int_{-T}^{T} e^{i(\omega - 2m\pi U_t/\delta)\tau} f_j \, d\tau \, dS(\vec{\eta}) \tag{16b}$$

where

$$\left.\begin{aligned} \alpha_1^{\pm} &= \frac{1}{\beta^2}(Mk \pm k_{m,n}) \\ \alpha_2^{\pm} &= 2m\pi/\delta \\ \alpha_3^{\pm} &= n\pi/b \end{aligned}\right\} \tag{17}$$

$$C^{\pm}_{m,n}(\vec{x}, \omega) = \frac{i}{2\pi\delta b} \frac{\cos\left(\frac{n\pi x_3}{b}\right)}{(1 + \delta_{n,0})k_{m,n}} \exp\left\{-i\left[\frac{1}{\beta^2}(Mk \pm k_{m,n})x_1 + \frac{2m\pi x_2}{\delta}\right]\right\} \tag{18}$$

and the plus sign corresponds to upstream propagation while the minus sign corresponds to downstream propagation. We shall first treat the quadrupole contribution P_Q to the pressure spectrum and then the dipole contribution P_D.

Quadrupole source model. - In order to use these results to predict the sound emission, it is necessary to determine the quadrupole source term $T_{ij}^{\dagger}$. As in any aeroacoustic problem, this is extremely difficult to do exactly since it requires a knowledge of the complete flow including the acoustic field. It is, therefore, usual to develop an approximate model for the source term. As a first step, it is usual in problems which do not involve combustion to replace Lighthill's stress tensor $T_{ij}^{\dagger}$ by the Reynolds stress. Thus, we assume

$$T_{ij}^{\dagger} = \rho_0 v_i^{\dagger} v_j^{\dagger} \tag{19}$$

We shall further assume that the relative velocity $v_i^{\dagger}$ can be decomposed into the sum of a solenoidal velocity u_i associated with the inlet flow distortion and a velocity w_i associated with the phase-locked rotor pressure field. Then w_i is independent of time in the $\vec{\eta}$-coordinate system, and u_i is independent of time in the $\vec{y}$-coordinate system. Hence,

$$v_i^{\dagger}(\vec{\eta}, t) = u_i(\vec{y}) + w_i(\vec{\eta}) \tag{20}$$

where u_i and w_i denote velocities relative to a coordinate system moving uniformly in the y_1-direction even though they are expressed as functions of the $\vec{y}$- and $\vec{\eta}$-coordinate systems, respectively.

Representation of distortion velocity. - Since $\vec{u}$ must be independent of time and since it must certainly be periodic in the y_2-direction, it can be represented by the Fourier series

$$\frac{\vec{u}}{U} = \sum_{q,s} \left[(\hat{i}A_{q,s} + \hat{j}B_{q,s}) \cos \frac{\pi s y_3}{b} + \hat{k}C_{q,s} \sin \frac{\pi s y_3}{b} \right] e^{2\pi i q y_2/\delta} \tag{21}$$

where $A_{q,s}$, $B_{q,s}$, and $C_{q,s}$ are complex constants and $\hat{i}$, $\hat{j}$, and $\hat{k}$ are unit vectors in the y_1-, y_2-, and y_3-directions, respectively. In order that $\vec{u}$ satisfy the solenoidal condition

$$\nabla \cdot \vec{u} = 0 \tag{22}$$

we must require that the coefficients $B_{q,s}$ and $C_{q,s}$ satisfy the condition

$$C_{q,s} + i\frac{2q}{s}\frac{b}{\delta}B_{q,s} = 0 \tag{23}$$

Notice that the normal component of each term in equation (21) automatically vanishes on the solid walls at $y_3 = 0$ and $y_3 = b$. Hence, no further restrictions need be imposed on the coefficients $A_{q,s}$ and $B_{q,s}$. Since the problem is linear, we need only calculate the sound generated by a single harmonic component

$$\frac{\vec{u}}{U} = \left[(\hat{i}A_{q,s} + \hat{j}B_{q,s})\cos\left(\frac{\pi s y_3}{b}\right) - \hat{k}i\frac{2qb}{s\delta}B_{q,s}\sin\left(\frac{\pi s y_3}{b}\right)\right]e^{2\pi i q y_2/\delta} \tag{24}$$

and the solution to the complete problem can be obtained by summing the results over q and s.

Rotor velocity field model. - We shall now develop an approximate model for the phase-locked rotor velocity field w_j. Most fans involve fairly small camber (especially at the tip, which is the critical region for producing sound), and thus linearized theory can be used. But since the quadrupole source is of interest at high subsonic Mach numbers, we must take into account the effects of compressibility. It is convenient to introduce the coordinate system which is alined with the blades as shown in figure 4. It is well known that the potential-flow field about such a blade row can be represented by a uniform velocity plus a distribution of line vortices along the blade chords. In order to simplify the analyses, we replace this vortex distribution by a discrete set of concentrated vortices lying at the midchord points. Let V_1 and V_2 denote the velocity components along the X_1- and X_2-directions, respectively (relative to the blades). Then according to linearized theory the velocity induced by a single compressible vortex of strength Γ_0 at the origin is given by (ref. 11)

$$V_1 - i\left(\frac{V_2}{\beta_r}\right) = \frac{\Gamma_0}{2\pi i}\frac{1}{Z}$$

where

$$\beta_r = \sqrt{1 - \left(\frac{U_r}{c_0}\right)^2} \tag{25}$$

$$Z = X_1 + i\beta_r X_2 \tag{26}$$

Hence, summing up this result over all blades shows that the concentrated vorticity approximation to the velocity field about the cascade is

$$V_1 - i\left(\frac{V_2}{\beta_r}\right) = U_r - i\left(\frac{v_0}{\beta_r}\right) + \frac{\Gamma_0}{2\pi i}\sum_{n=-\infty}^{\infty} \frac{1}{Z - i\Delta_0 n} \tag{27}$$

where v_0 is a uniform (in general) complex velocity which will be chosen to make the flow far upstream of the cascade equal to U_r and

$$\Delta_0 = \Delta(\beta_r \cos \gamma - i \sin \gamma) \tag{28}$$

where Δ is the interblade spacing and γ is called the stagger angle. But upon using the relation

$$\sum_{n=-\infty}^{\infty} \frac{1}{Z - in\pi} = \coth Z$$

equation (27) becomes

$$V_1 - i\left(\frac{V_2}{\beta_r}\right) = U_r - i\left(\frac{v_0}{\beta_r}\right) + \frac{\Gamma_0}{2i\Delta_0} \coth \frac{\pi Z}{\Delta_0}$$

And since

$$\lim_{x_1 \to -\infty} \coth \frac{\pi Z}{\Delta_0} = -1$$

we must put

$$\frac{v_0}{\beta_r} = \frac{\Gamma_0}{2\Delta_0}$$

Hence,

$$V_1 - i\left(\frac{V_2}{\beta_r}\right) = U_r + \frac{\Gamma_0}{2i\Delta_0}\left(1 + \coth\frac{\pi Z}{\Delta_0}\right) \tag{29}$$

It can be seen from figure 4 that the X_1, X_2 coordinate system is related to the rotating η_1, η_2 duct-alined coordinates by

$$X_1 = \eta_1 \cos\gamma + \eta_2 \sin\gamma$$

$$X_2 = -\eta_1 \sin\gamma + \eta_2 \cos\gamma$$

Hence, it follows from equations (26) and (28) that

$$\frac{Z}{\Delta_0} = \frac{\eta_1(\cos\gamma - i\beta_r \sin\gamma)}{\Delta(\beta_r \cos\gamma - i \sin\gamma)} + i\frac{\eta_2}{\Delta}$$

$$= \frac{\eta_1\left[\beta_r + i\left(1 - \beta_r^2\right)\sin\gamma\cos\gamma\right]}{\Delta\left(\beta_r^2\cos^2\gamma + \sin^2\gamma\right)} + i\frac{\eta_2}{\Delta}$$

But upon using the velocity triangle in figure 4, this can be written as

$$\frac{Z}{\Delta_0} = \frac{z}{\Delta} \tag{30}$$

where

$$z = \eta_1 D + i\eta_2 \tag{31}$$

$$D \equiv \frac{\beta_r + iMM_t}{\beta^2} \tag{32}$$

and

$$M_t = \frac{U_t}{c_0} \tag{33}$$

is the Mach number of the blade row. Now the velocity components w_1 and w_2 are in the η_1- and η_2-directions and are measured relative to a reference frame moving with a uniform velocity U in the η_1-direction, while the velocities V_1 and V_2 are in the X_1- and X_2-directions and are measured in a reference frame moving with the cascade velocity U_t. Hence, it follows from figure 4 that

$$V_1 = (w_1 + U) \cos \gamma + (w_2 + U_t) \sin \gamma$$

and

$$V_2 = (w_2 + U_t) \cos \gamma - (w_1 + U) \sin \gamma$$

$$= w_2 \cos \gamma - w_1 \sin \gamma$$

Then

$$(\beta_r \cos \gamma - i \sin \gamma)\left[V_1 - i\left(\frac{V_2}{\beta_r}\right) - U_r\right] = \frac{w_1\beta^2 - iw_2\overline{D}}{\beta_r}$$

Hence, multiplying equation (29) through by $(\beta_r \cos \gamma - i \sin \gamma)$ and using equations (28) and (30) shows that

$$\beta^2(w_1 - iw_2\overline{D}) = \frac{\Gamma_0\beta_r}{2i\Delta}\left(1 + \coth \frac{\pi z}{\Delta}\right) \tag{34}$$

But since

$$\lim_{\eta_1 \to +\infty} \beta^2\left(w_1 - iw_2\overline{D}\right) = \frac{\Gamma_0}{i\Delta}\ \beta r$$

equating the imaginary parts of this expression shows that Δw_2, the change in w_2 across the blade row, is related to Γ_0 by

$$\frac{\Gamma_0}{\Delta} = \Delta w_2 = -U_t\theta$$

where $\theta = -\Delta w_2/U_t$ is called the work coefficient of the fan. Hence, equation (34) can be

written as

$$\beta^2(w_1 - iw_2\overline{D}) = \frac{i\theta\beta_r U_t}{2}\left(1 + \coth\frac{\pi z}{\Delta}\right)$$

$$= \frac{i\theta\beta_r U_t}{2}\frac{e^{\pi z/\Delta}}{\sinh\frac{\pi z}{\Delta}}$$

By using the geometric series

$$\frac{1}{1 - Z} = \sum_{p=0}^{\infty} Z^p \qquad \text{for} \quad |Z| < 1$$

(with $Z \rightarrow \exp(\pm 2\pi Z/\Delta)$), this becomes

$$\beta^2(w_1 - iw_2\overline{D}) = \begin{cases} -iU_t\beta_r\theta \sum_{p=1}^{\infty} e^{2\pi pz/\Delta} & \text{if } \eta_1 < 0 \\ iU_t\beta_r\theta \sum_{p=0}^{\infty} e^{-2\pi pz/\Delta} & \text{if } \eta_1 > 0 \end{cases}$$

Equating real and imaginary parts now shows that

$$w_1\beta^2 - w_2 MM_t = \frac{-iU_t\theta\beta_r}{2}\sum_{p=1}^{\infty}(e^{2\pi pz/\Delta} - e^{2\pi p\overline{z}/\Delta}) \qquad \text{for} \quad \eta_1 < 0$$

$$w_2 = \frac{U_t\theta}{2}\sum_{p=1}^{\infty}(e^{2\pi pz/\Delta} + e^{2\pi p\overline{z}/\Delta}) \qquad \text{for} \quad \eta_1 < 0 \tag{35}$$

or adding the results

$$w_1 = \frac{-iU_t\theta}{2}\sum_{p=1}^{\infty}(De^{2\pi pz/\Delta} - \overline{D}e^{2\pi p\overline{z}/\Delta}) \qquad \text{for} \quad \eta_1 < 0 \tag{36}$$

The noise generated by inlet flow distortion probably has its largest effect on the sound field passing through the fan inlet. We shall therefore restrict our attention to the upstream-propagating waves. We shall also suppose that only the front half of the cascade potential-flow field is effective in interacting with the inlet distortion and generating sound which propagates upstream. Hence, we set

$$w_1 = w_2 = 0 \qquad \text{for } \eta_1 > 0 \tag{37}$$

Evaluation of quadrupole source term. - The results of the previous two subsections can be used to evaluate the source term $Q^+_{m,n}$ in equation (15a). Thus, using equation (12) to eliminate y_i in equation (24) and inserting the result in equations (19) and (20) shows that equation (16a) becomes, upon carrying out the integration with respect to η_3 (since only the cross terms $w_i u_j$ can contribute to the sound field - the other terms representing steady flows in a inertial reference frames),

$$Q^+_{m,n} = -bU(1 + \delta_{s,0})\delta_{s,n}\rho_0\alpha^+_\sigma E_{m,n} \int_{-\infty}^{0}\int_{0}^{\delta} \exp\left\{i\left[\alpha^+_1\eta_1 + \frac{2\pi}{\delta}(q + m)\eta_2\right]\right\} w_\sigma \, d\eta_2 \, d\eta_1$$

$$\times \int_{-T}^{T} \exp\left\{i\left[\omega - \frac{2\pi U_t}{\delta}(m + q)\right]\tau\right\} d\tau \tag{38}$$

where (since $w_3 = 0$) the repeated Greek index σ takes on only the values 1 and 2 and

$$E_{m,n}(k) \equiv \alpha^+_1 A_{q,s} + \alpha^+_2 B_{q,s} + \frac{\alpha^+_3 2q}{s}\frac{b}{\delta} B_{q,s}$$

Hence, it follows from equation (17) that when $n = s$

$$E_{m,s}(k) = \frac{2\pi(m + q)}{\delta} B_{q,s} + \frac{(Mk + k_{m,s})}{\beta^2} A_{q,s} \tag{39}$$

Carrying out the integration with respect to τ and taking the limit as $T \to \infty$ now shows, since $\lim_{T\to\infty} \int_{-T}^{T} e^{i\tau\beta} \, d\tau = 2\pi\delta(\beta)$, that

$$Q^{+}_{m,n} = -b(1 + \delta_{s,0})U\delta_{s,n}2\pi\,\delta\left(\omega - \frac{2\pi U_t}{\delta}(m + q)\right)\rho_0\alpha^{+}_{\sigma}$$

$$\times E_{m,s}\int_{-\infty}^{0}\int_{0}^{\delta}\exp\left\{i\left[\alpha^{+}_{1}\eta_1 + \frac{2\pi}{\delta}(q + m)\eta_2\right]\right\}w_{\sigma}\,d\eta_2\,d\eta_1$$

Inserting equations (17), (35), and (36) into this result and carrying out the integrations with respect to η_1 and η_2 show that

$$Q^{+}_{m,n} = \begin{cases} b\delta\rho_0 U_t\theta(1 + \delta_{s,0})\delta_{s,n}U\pi\delta\left(\omega - \dfrac{2\pi U_t}{\delta}(m + q)\right)E_{m,s}\left[\dfrac{iD\alpha^{+}_{1} - \dfrac{2\pi m}{\delta}}{i\alpha^{+}_{1} - \dfrac{2\pi}{\delta}(m + q)D}\right] \\ \qquad\qquad \text{if } \dfrac{m + q}{B} = -1, -2, -3, \ldots \\ 0 \quad \text{if } \dfrac{m + q}{B} \neq \pm 1, \pm 2, \ldots \\ -b\delta\rho_0 U_t\theta(1 + \delta_{s,0})\delta_{s,n}U\pi\delta\left(\omega - \dfrac{2\pi U_t}{\delta}(m + q)\right)E_{m,s}\left[\dfrac{\overline{iD\alpha_1 - \dfrac{2\pi m}{\delta}}}{i\alpha^{+}_{1} - \dfrac{2\pi}{\delta}(m + q)D}\right] \\ \qquad\qquad \text{if } \dfrac{m + q}{B} = 1, 2, 3, \ldots \end{cases} \tag{40}$$

where the overbar denotes the complex conjugate. Substituting equation (40) into equation (15a) and changing the index of summation from m to $m + q$ now shows that

$$P_Q(\omega) = b\delta\rho_0 U_t U\theta(1 + \delta_{s,0})\pi\sum_{\substack{p=-\infty \\ p\neq 0}}^{\infty}\delta\left(\omega - \frac{2\pi U_t}{\Delta}p\right)C^{+}_{pB-q,s}(\vec{x})$$

$$\times H^{(0)}_{p,q,s}E_{pB-q,s}\left(\frac{2\pi M_t p}{\Delta}\right) \tag{41}$$

$$H^{(0)}_{p,q,s} \equiv \begin{cases} -\overline{H}_{p,q,s} & \text{for } p > 0 \\ H_{p,q,s} & \text{for } p < 0 \end{cases} \tag{42}$$

$$H_{p,q,s} \equiv \frac{\left(p - \frac{q}{B}\right)\beta^2 - iD(MM_t p + K_{p,q,s})}{p\beta_r - iK_{p,q,s}} \tag{43}$$

and (see eq. (10))

$$K_{p,q,s} \equiv \frac{\Delta}{2\pi} k_{pB-q,s}\left(\frac{2\pi M_t p}{\Delta}\right)$$

$$= \sqrt{p^2 M_t^2 - \beta^2\left[\left(p - \frac{q}{B}\right)^2 + \left(\frac{s\Delta}{2b}\right)^2\right]} \tag{44}$$

The pressure spectrum for an arbitrary flow distortion can now be obtained by summing equation (41) over all s and q to obtain

$$P_Q(\omega) = \pi b\delta\rho_0 U_t U\theta \sum_{s,q}(1 + \delta_{s,0}) \sum_{\substack{p=-\infty \\ p\neq 0}}^{\infty} \delta\left(\omega - \frac{2\pi p U_t}{\Delta}\right) C^{+}_{pB-q,s}(\vec{x})$$

$$\times H^{(0)}_{p,q,s} E_{pB-q,s}\left(\frac{2\pi M_t p}{\Delta}\right) \tag{41a}$$

This is the formula for the quadrupole source contribution to the pressure spectrum. The principal assumptions on which it is based are discussed in the section Quadrupole source model.

Dipole Sound

We shall now calculate the contribution of the dipole source to the pressure field.

Evaluation of dipole source term for periodic forces. - It is usual practice when dealing with dipole sound from fans and propellers to neglect the variation in the retarded time $\alpha_1^{\pm}\eta_1$ between the surface of the blades and the rotational plane of the cascade (which we take to be the $\eta_1 = 0$ plane). It is also reasonable to neglect the blade forces in the (radial) η_3-direction. Then it is shown in reference 11 that the integration in equation (16b) over the blade surface can be reduced to an integral over the rotational plane of the cascade to obtain (after carrying out the differentiation with respect to η_j)

$$D^{\pm}_{m,n}(\omega) = i\alpha^{\pm}_{\sigma} \int_{y_1=0} e^{i\alpha_2^{\pm}\eta_2} \cos \alpha_3^{\pm}\eta_3 \int_{-T}^{T} e^{i(\omega - 2m\pi U_t/\delta)\tau} \tilde{f}_{\sigma}\, d\tau\, d\eta_2\, d\eta_3 \tag{45}$$

where, as before, the Greek index σ only takes on the values 1 and 2 and $\tilde{f}_{\sigma}(\eta_1, \eta_3)$ is the σ^{th} component of the net blade force per unit projected area (on the rotational plane) acting on the cascade at the point η_2, η_3 of the rotational plane.

Since it is assumed that the inlet flow distortion is steady, the unsteady blade forces due to the passage of the blades through this distortion must certainly be periodic, with frequency equal to the shaft rotational frequency

$$\Omega = \frac{2\pi U_t}{\delta} \tag{46}$$

Hence, we can expand these forces in a Fourier series to obtain

$$\tilde{f}_{\sigma} = \sum_{q=-\infty}^{\infty} F_q^{\sigma}(\eta_2, \eta_3) e^{-iq\Omega\tau} \tag{47}$$

where

$$F_q^{\sigma} = \frac{\Omega}{2\pi} \int_0^{(2\pi/\Omega)} e^{iq\Omega\tau} \tilde{f}_{\sigma}\, d\tau \tag{48}$$

Upon inserting this into equation (45), carrying out the integration with respect to τ, and taking the limit as $T \to \infty$, we get

$$D^{\pm}_{m,n}(\omega) = i\alpha^{\pm}_{\sigma} 2\pi \sum_{q=-\infty}^{\infty} \delta\left(\omega - (m+q)\Omega\right) \int_A e^{i\alpha_2^{\pm}\eta_2} \cos(\alpha_3^{\pm}\eta_3) F_q^{\sigma}\, d\eta_2\, d\eta_3 \tag{49}$$

Inserting this result into equation (15b) and shifting the index of summation from m to $p = m + q$ and using equation (17) show that

$$P_D(\omega) = 2\pi i \sum_{n=0}^{\infty} \sum_{p,\, q=-\infty}^{\infty} \delta(\omega - p\Omega) C^{(0)}_{p,\, q,\, n}(\vec{x}) \int_A e^{i2\pi(p-q)\eta_2/\delta} \cos\left(\frac{n\pi\eta_3}{b}\right)$$

$$\times \left\{ \frac{2\pi(p - q)}{\delta} F^2_q + \frac{1}{\beta^2} \left[\frac{2\pi M M_t}{\delta} p \pm k_{p-q,\, n}(\Omega p) \right] F^1_q \right\} d\eta_2\, d\eta_3 \qquad (50)$$

where

$$C^{(0)}_{p,\, q,\, n}(\vec{x}) \equiv C^{\pm}_{p-q,\, n}(\vec{x}, \Omega p) \qquad (51)$$

Case of identical blades. - When the fan consists of B identical blades, the unsteady force acting on each blade must be the same as on any other blade whenever it passes through the same position of the inlet disturbance. Hence, the force $\tilde{f}_\sigma$ can be expressed in terms of the individual blade force f^0_σ by

$$\tilde{f}_\sigma = \sum_{s=1}^{B} f^0_\sigma \left(\eta_3,\ \eta_2 + \frac{\delta}{B}(s - 1),\ \tau + \frac{2\pi}{\Omega B}(s - 1) \right)$$

Inserting this into equation (48) and shifting the variable of integration implies that

$$F^\sigma_q = \sum_{s=1}^{B} e^{-2\pi i(s-1)q/B} F^0_{\sigma,\, q}\left(\eta_3,\ \eta_2 + \frac{\delta}{B}(s - 1) \right) \qquad (52)$$

where

$$F^0_{\sigma,\, q} \equiv \frac{\Omega}{2\pi} \int_0^{2\pi/\Omega} e^{iq\Omega\tau} f^0_\sigma(\eta_2,\ \eta_3,\ \tau)\, d\tau \qquad (53)$$

is simply the q^{th} Fourier coefficient of the force f^0_σ acting on an individual blade.

Substituting equation (52) into equation (50), shifting the variable of integration from η_2 to $\eta_2 + (\delta/B)(s - 1)$, and noting that

$$\sum_{s=1}^{B} e^{-2\pi ip(s-1)/B} = \begin{cases} B \text{ for } p = 0, \pm B, \pm 2B, \ldots \\ 0 \text{ for } p \neq 0, \pm B, \pm 2B, \ldots \end{cases}$$

show that

$$P_D(\omega) = 2\pi iB \sum_{n=0}^{\infty} \sum_{p,q=-\infty}^{\infty} \delta(\omega - pB\Omega) C^{(0)}_{pB,q,n}(\vec{x})$$

$$\times \int_{A_0} e^{i2\pi(pB-q)\eta_2/\delta} \cos\left(\frac{n\pi\eta_3}{b}\right) \left\{ \frac{2\pi(pB-q)}{\delta} F^0_{2,q} + \frac{1}{\beta^2}\left[\frac{2\pi MM_t p}{\Delta} \pm k_{pB-q,n}(\Omega pB)\right] F^0_{1,q} \right\} d\eta_2 \, d\eta_3 \tag{54}$$

where we now need only carry out the integration over the projected area A_0 of a single blade.

Dipole source model. - We now encounter the same difficulty as occurred with the quadrupole term. Namely, the blade force f^0_σ, which must be known in order to calculate the sound field, is, in general, a complicated function whose exact determination requires a knowledge of the complete flow, including the sound field. We shall again proceed by developing an approximate model for this term. Although it is now possible to obtain a fairly sophisticated model for f^0_σ, we shall adopt the relatively simple model that is conventionally used in the literature. Thus, we suppose that f^0_σ is concentrated at the centerline of the blade (which we can suppose lies at $\eta_2 = 0$). We shall also suppose that the viscous contributions can be neglected. Then f^0_σ can be expressed in terms of the fluctuating lift force per unit span l acting on the blade and the stagger angle γ defined in figure 4 by[2]

$$\tilde{f}^0_2 = -\delta(\eta_2) l \cos\gamma$$

$$\tilde{f}^0_1 = \delta(\eta_2) l \sin\gamma$$

Inserting the result into equation (52) now shows that

[2]Recall that $\tilde{f}^0_\sigma$ denotes a force exerted on the fluid while l denotes a force exerted on the blades.

$$\left.\begin{aligned} F^0_{2,q} &= -\delta(\eta_2)L_q \cos\gamma \\ F^0_{1,q} &= \delta(\eta_2)L_q \sin\gamma \end{aligned}\right\} \tag{55}$$

where L_q denotes the q^{th} Fourier coefficient of the lift force per unit span acting on an individual blade.

Up to this point the assumptions have been fairly mild. However, we must now determine L_q from a knowledge of the coefficients of the flow distortion entering the fan. We shall restrict our attention to the case where the flow distortion is only in the axial velocity so that $B_{q,s} = C_{q,s} = 0$. Since the quadrupole term dominates the dipole at sufficiently high Mach numbers, we shall not take into account compressibility in calculating L_q. In addition, suppose (1) that each airfoil in the cascade acts individually and is uninfluenced by the remaining blades, (2) that it responds locally in a two-dimensional manner so that strip theory can be applied, and (3) that the camber is small enough so that linearized thin-airfoil theory applies.

Then, as is shown in reference 10, L_q can be calculated from the Fourier coefficients in equation (21) and the Sears' function $S(\sigma_q)$ by

$$L_q = -\pi c \rho_0 U_r U \sin\gamma S(\sigma_q) \sum_{s=0}^{\infty} A_{q,s} \cos\frac{\pi s \eta_3}{b} \tag{56}$$

where c is the airfoil chord, $S(\sigma_q)$ is the Sears' function, and

$$\sigma_q \equiv \frac{q\Omega c}{2U_r} \tag{57}$$

is the reduced frequency. The Sears' function can be expressed in terms of Bessel functions. However, it is well known that it can be approximated quite accurately for almost all frequencies by the relation

$$S(\sigma_q) \approx \frac{\exp\left\{-i\sigma_q\left[1 - \dfrac{\pi^2}{2(1 + 2|\sigma_q|)}\right]\right\}}{\sqrt{1 + 2\pi|\sigma_q|}} \tag{58}$$

We shall adopt this approximation herein. Bender (ref. 12) has recently shown that in the case of a flat plate the correction for finite length in the y_3-direction can be approximated fairly accurately by multiplying equation (56) by the ratio of the steady-state lift slope $dC_L/d\alpha$ (the lift slope for infinite-span thin airfoils) to 2π. Upon the adopting of this correction, equation (56) becomes

$$L_q = -c\frac{\rho_0}{2}\frac{dC_L}{d\alpha}U_r U \sin\gamma S(\sigma_q)\sum_{s=0}^{\infty} A_{q,s}\cos\frac{\pi s\eta_3}{b} \tag{59}$$

The lift-slope $dC_L/d\alpha$ is a function primarily of the aspect ratio AR of the blades

$$AR \equiv \frac{b}{c} \tag{60}$$

Finally, it is shown in reference 13 that $dC_L/d\alpha$ can be approximated by the relation

$$\frac{dC_L}{d\alpha} = \frac{2\pi\ AR}{AR + 2\left(\frac{AR + 4}{AR + 2}\right)} \tag{61}$$

Using the relations (shown in fig. 4)

$$\sin\gamma = \frac{U_t}{U_r}$$

$$\cos\gamma = \frac{U}{U_r}$$

substituting equation (59) into equation (55), using the result in equation (54), and carrying out the integrations show

$$P_D(\omega) = \pi i b B \Delta \rho_0 U_t U \left(\frac{1}{2}\frac{dC_L}{d\alpha}\frac{c}{\Delta}\frac{c_0}{U_r}\right)\sum_{s,q}(1+\delta_{s,0})\sum_{p=-\infty}^{\infty}\delta\left(\omega - \frac{2\pi U_t}{\Delta}p\right)C^{(0)}_{pB,q,n}(\vec{x})S(\sigma_q)$$

$$\times\left[\frac{2\pi(pB-q)}{\delta}M - \frac{1}{\beta^2}\left(\frac{2\pi M M_t}{\Delta}p \pm k_{pB-q,s}\right)M_t\right]A_{q,s} \qquad (62)$$

Evaluation of Pressure Field Due to Individual Tones

At this point, we shall restrict our attention to upstream propagation for the case where the flow distortion is purely in the axial direction. Then inserting equations (41a) and (62) into equation (14a) and using the result in equation (14) show that the pressure field only contains frequencies which are multiples of the blade passing frequency and that the p^{th} harmonic of the pressure fluctuation p'_p is

$$p'_p = \frac{2bB\rho_0\pi^2 U_t U}{\beta^2}\exp\left(\frac{-2\pi U_t}{\Delta}pt\right)\sum_{s,q}(1+\delta_{s,0})C^{(0)}_{pB,q,s}(\vec{x})\Theta_{p,q,s}A_{q,s} \qquad (63)$$

where we have used equations (39) and (44) and put

$$\Theta_{p,q,s} \equiv \theta(MM_t p + K_{p,q,s})H^{(0)}_{p,q,s} + i\psi S(\sigma_q)\left[\frac{M(pB-q)}{B}\beta^2 - M_t(MM_t p + K_{p,q,s})\right] \qquad (64)$$

and

$$\psi \equiv \frac{1}{2}\frac{dC_L}{d\alpha}\left(\frac{c}{\Delta}\right)M_r^{-1} \qquad (65)$$

Radiated Acoustic Power

The quantity which is perhaps of most interest is the total acoustic power $\mathcal{P}_p$ radiated upstream in the p^{th} harmonic. This can be calculated by integrating the axial component $\bar{I}_p(\vec{x})$ of the sound intensity in the p^{th} harmonic over the cross-sectional

area of the duct. Thus,[3]

$$\mathscr{P}_p = \lim_{x_1 \to -\infty} 2 \int_0^{\delta} \int_0^{b} \overline{I}_p(\vec{x})\, dx_2\, dx_3 \quad \text{for } p=1,2,\ldots \tag{66}$$

It is shown in reference 11 that

$$\overline{I}_p = (1 + M^2) p'_p v_p + \frac{M}{\rho_0 c_0} |p'_p|^2 + \rho_0 c_0 M |v_p|^2 \tag{67}$$

where v_p is the p^{th} harmonic of the acoustic velocity and is related to p'_p by

$$\frac{-\partial p'_p}{\partial x_1} = -\rho_0 c_0 \left(i \frac{2\pi M_t}{\Delta} p - M \frac{\partial}{\partial x_1} \right) v_p$$

Hence, inserting equations (18) and (63) into this relation (with $k = 2\pi M_t p/\Delta$) shows that

$$v_p = \frac{2bBU_t U\pi^2}{c_0 \beta^2} e^{-2\pi p U_t t/\Delta} \sum_{s,q} \lambda_{s,q} (1 + \delta_{s,0}) C^{(0)}_{pB,q,s}(\vec{x}) \Theta_{p,q,s} A_{q,s} \tag{68}$$

where

$$\lambda_{s,q} = - \frac{MM_t p + K_{p,q,s}}{M_t p + MK_{p,q,s}} \tag{69}$$

Since equation (18) shows that

$$\int_0^{\delta} \int_0^{b} C_{m,n} \overline{C}_{m',n'}\, dx_2\, dx_3 = \frac{\delta_{m,m'} \delta_{n,n'}}{8\pi^2 \delta b k^2_{m,n} (1 + \delta_{n,0})}$$

substituting equations (63) and (68) into equation (67) and using the result in equation (66) shows that

---

[3]The factor 2 arises because both $\overline{I}_p$ and $\overline{I}_{-p}$ contribute to the acoustic power in the p^{th} tone.

$$\frac{\mathscr{P}_p}{\rho_0 c_0^3 Bb\Delta} = \frac{(MM_t)^2 pM_t}{4}$$

$$\times \sum_{\substack{\text{all } q \text{ and all } s \geq 0 \text{ with} \\ p^2M_t^2 > \beta^2\left[\left(p - \frac{q}{B}\right)^2 + \left(\frac{s}{2b}\right)^2\right]}} (1 + \delta_{s,0}) \frac{|\Theta_{p,q,s}|^2 |A_{q,s}|^2}{(M_t p + MK_{p,q,s})^2 K_{p,q,s}} \tag{70}$$

For convenient reference we also note that

$$H_{p,q,s} = \frac{\left(p - \frac{q}{B}\right)\beta^2 - iD(MM_t p + K_{p,q,s})}{p\beta_r - iK_{p,q,s}} \tag{43}$$

$$K_{p,q,s} = \sqrt{p^2M_t^2 - \beta^2\left[\left(p - \frac{q}{B}\right)^2 + \left(\frac{s\Delta}{2b}\right)^2\right]} \tag{44}$$

$$\Theta_{p,q,s} \equiv -\theta\overline{H}_{p,q,s}(MM_t p + K_{p,q,s}) + i\psi S(\sigma_q)\left[\frac{M(pB - q)}{B}\beta^2 - M_t(MM_t p + K_{p,q,s})\right] \tag{71}$$

$$\psi = \frac{1}{2M_r}\left(\frac{c}{\Delta}\right)\left[\frac{2\pi\, AR}{AR + 2\left(\frac{AR + 4}{AR + 2}\right)}\right] \tag{72}$$

$$S(\sigma_q) = \frac{\exp\, -i\sigma_q\left[1 - \frac{\pi^2}{2(1 + 2\pi|\sigma_q|)}\right]}{\sqrt{1 + 2\pi|\sigma_q|)}} \tag{58}$$

$$\sigma_q = \frac{q\pi M_t}{BM_r}\left(\frac{c}{\Delta}\right) \tag{73}$$

Equation (71) was obtained by combining equations (42) and (64), equation (72) was obtained by combining equations (65) and (61), and equation (73) was obtained by combining equations (57) and (46).

Calculation of Distortion Coefficients

In order to use equation (70) to predict the radiated sound power, it is necessary to determine the Fourier coefficients $A_{q,s}$. But it follows from equation (21) that these coefficients can be determined from the axial distortion velocities u_1 by the relation

$$A_{q,s} = \frac{2}{b\delta(1 + \delta_{s,0})} \int_0^b \int_0^\delta e^{-2\pi i q y_2/\delta} \cos\left(\frac{\pi s y_3}{b}\right) \frac{u_1(y_2, y_3)}{U} \, dy_3 \, dy_2 \tag{74}$$

It is convenient to suppose that the distortion velocity can be expressed as the product

$$\frac{u_1}{U} = I \, f(y_2) \, g(y_3) \tag{75}$$

then

$$A_{q,s} = I a_q \, d_s$$

where

$$a_q = \frac{1}{\delta} \int_0^\delta e^{-2\pi i q y_2/\delta} f(y_2) \, dy_2$$

and

$$d_s = \frac{2}{b(1 + \delta_{s,0})} \int_0^b \cos\left(\frac{\pi s y_3}{b}\right) g(y_3) \, dy_3$$

When the flow distortion can be represented by N Gaussian profiles (for $N = 1, 2, \ldots$) in the circumferential direction (see fig. 5(a) for the case where $N = 2$),

$$f(y_2) = \exp\left[\frac{-\left(\frac{y_2}{\delta} - \frac{1+2j}{2N}\right)^2}{(\sigma')^2}\right] \left\{ \left[\frac{j\delta}{N} < y_2 < \frac{(j+1)}{N}\delta\right] \text{ for } j = 0, 1, \ldots, N-1 \right. \tag{76}$$

we find that[4]

$$a_q = \begin{cases} \sqrt{\pi} N\sigma' e^{\frac{-i\pi}{N}q} e^{-\pi^2 q^2 (\sigma')^2} \; Re\, \mathrm{erf}\left(\frac{1}{2N\sigma'} + \pi i q \sigma'\right) & \text{for } q = 0, \pm N, \pm 2N, \ldots \\ 0 \quad \text{otherwise} \end{cases} \tag{77}$$

When the flow distortion is a square wave in the circumferential direction (fig. 5(b)),

$$f(y_2) = \begin{cases} 1 & \text{for } \left|\frac{y_2}{\delta} - \frac{1}{2}\right| < \sigma'' \\ 0 & \text{for } \left|\frac{y_2}{\delta} - \frac{1}{2}\right| > \sigma'' \end{cases} \tag{78}$$

and we find that

$$a_q = \frac{(-1)^q}{\pi q} \sin 2\pi q \sigma'' \tag{79}$$

When the flow distortion is uniform in the radial direction

$$g(y_3) = 1 \tag{80}$$

we find that

$$d_s = \delta_{s,0} \tag{81}$$

And when the flow distortion is a square wave concentrated around the tip region

[4] If σ' gets large, the Gaussians will merge but, of course, still remain periodic.

$$g(y_3) = \begin{cases} 1 & \text{for } 1 - \tilde{\sigma} < \dfrac{y_3}{b} \leq 1 \\ 0 & \text{for } 0 \leq \dfrac{y_3}{b} < 1 - \tilde{\sigma} \end{cases} \tag{82}$$

we find that

$$d_s = \frac{(-1)^s 2}{\pi s(1 + \delta_{s,0})} \sin \pi s\tilde{\sigma} \tag{83}$$

RESULTS AND DISCUSSION

Parameters in Solution

Equations (70) to (73) can be used to calculate the total sound power radiated upstream in the p^{th} harmonic of the BPF tone which results from the interaction of the rotors with an axial inlet flow distortion. In order to do this, it is necessary to know the axial distortion velocity u_1 entering the fan. The geometry of the fan is characterized by the parameters c, b, B, and Δ. They denote the blade chord, the blade height, the number of blades, and the interblade spacing. The remaining parameters which appear in equation (70) depend on the operating conditions of the fan. They are the cascade velocity (tip speed) U_t, the throughflow (axial) velocity U, and the work coefficient θ. The work coefficient is a measure of the loading on the fan.

Dipole and Quadrupole Contributions

The first term in equation (71) represents the quadrupole contribution to the radiated sound power, while the second term represents the dipole contribution. These terms will not always be additive but can easily be out of phase and produce a sound field which is less than that which would be produced by either one alone. It follows from equations (71) and (72) that the ratio of the quadrupole term to the dipole term is proportional to the ratio of the work coefficient θ to the cascade solidity c/Δ. Thus, the quadrupole contribution will tend to dominate for highly loaded, low-solidity blades. The dipole contribution is independent of the work coefficient.

Numerical Results

The dimensionless radiated sound power in the first tone due to a localized flow distortion has been calculated for values of the fan design parameters covering a range corresponding to the various quiet fans tested at the Lewis Research Center.

It is assumed that the flow distortion consists of a single pulse with a Gaussian shape in the circumferential direction and is a square wave in the radial direction (i.e., a combination of eq. (76) with $N = 1$ and eq. (82)). It has been found, that for narrow distortions, the detailed shape of the pulse has little effect on the radiated sound and only its size is important. Equations (70), (74), and (75) show that the radiated sound power varies as the square of the normalized distortion velocity.

The plots show the variation in radiated power in the fundamental tone as the rotor circumferential Mach number is varied while the ratio of axial to rotor circumferential Mach number is kept equal to 1/2. Most quiet fans tested at Lewis correspond to this case when operated along a fixed throttle line which passes through the design point. When fans are operated in this manner, the work coefficient θ tends to remain fairly constant. In fact, the work coefficient varies little from fan to fan and is roughly equal to 0.4.

Figure 6 illustrates the effect of changing the number of blades while holding the cross-sectional area of the fan constant. It can be seen from the figure that the effect is very small (of the order of about 2 dB) over the range considered.

Figure 7 shows the effect of changing the circumferential size of the distortion. The distortion width is $2\sigma'\delta$. It can be shown from the figure that for very small distortions the sound power varies roughly as M_t to the sixth power, while (at least for this case) when the distortion becomes about equal to the blade spacing, the tone power varies as the velocity to the eighth power. The fans tested at Lewis exhibit anywhere from a velocity-to-the-fifth-power relation to a velocity-to-the-eighth-power relation (see fig. 20 of ref. 4). As the size of the distortion increases further, the rate of increase of the radiated tones with velocity becomes greater. This is due to the fact that the inlet distortion contains predominantly lower order harmonics which generate acoustic modes which are cut off at the lower Mach numbers. Notice that at each Mach number there is a certain distortion size which maximizes the noise.

Comparison with Experimental Data

The predictions of the analytical results have been compared with various fans tested at Lewis. The first comparison is with a 51-centimeter (20-in.) diameter model fan rotor tested in an indoor compressor aerodynamic performance rig. The results of

these tests are reported in reference 14. This fan, designated rotor 1 - model 1, is shown in figure 8. The relevant design parameters and operating conditions are listed in table I. The latter correspond to the highest subsonic speeds at which the fans were tested. The flow distortion entering the fan has not been measured. However, there are four support struts ahead of the fan. Downstream of the struts there is a large contraction of the flow to the 51-centimeter (20-in.) diameter fan size. We therefore assume that the flow distortion can be represented by four equally spaced Gaussian profiles in the circumferential direction, where the width is equal to the thickness of the struts, and that it is uniform in the radial direction. The amplitude of the distortion is unknown, but a maximum value of $1\frac{1}{2}$ percent of the free-stream axial velocity is not unreasonable. The comparison between the experiment and theory is shown in figure 9. Since the amplitude of the flow distortion has not been measured, the absolute level of these curves has to be regarded as uncertain. Indeed the assumption of $1\frac{1}{2}$ percent distortion is equivalent to putting the theoretical curves through a single data point. However, it can be seen that the theory certainly predicts the correct trends. The triangular points show the contribution of the quadrupole source to the sound power. It can be seen that at the center of the 80-percent-speed curve the quadrupole is the dominant contribution, while for the 60-percent-speed curve the largest contribution is from the dipole source. The dropoff at the high-Mach-number end of each of the constant-speed curves occurs because of the dropoff in the dominant quadrupole source. The dipole term tends to decrease monotonically with decreasing relative Mach number.

The analysis was also compared with front-quadrant fundamental tone measurements taken in several subsonic full-scale fans in the installation shown in figure 10. The concrete support structure in this installation is believed to be the cause of an inlet flow distortion entering the fan. This distortion was measured for the QF-3 fan in reference 7. By using this measured flow distortion data as an input to the analysis, the fundamental BPF tone is predicted. This prediction is compared with measurements on a number of fans operated subsonically on this rig. The relevant design parameter and operating conditions are shown in table II. All the fans were nominally 1.8 meters (6 ft) in diameter.

In carrying out the comparison, it is assumed that the flow distortion is the same for all fans as it was for the QF-3 fan (operated at 90 percent speed) for which the measurements were taken. The measurements of reference 8 showed that a small region of high velocity existed at the bottom center of the inlet. This distortion is modeled analytically by a Gaussian profile in the circumferential (y_2) direction and a step profile in the radial (y_3) direction. The measured distortion was found to cover 10° in the circumferential direction. Hence, we take the ratio $2\sigma'$ of the width of the Gaussian to the circumference to be $10^\circ/360^\circ$, or 0.139. The radial extension of the distortion was about 8.9 centimeters ($3\frac{1}{2}$ in.). Hence, the ratio $\tilde{\sigma}$ of the height of the distortion to

the blade height is taken to be 3.5/19.35 or 0.18. By using these data, numerical results have been calculated for the fans listed in table II. The results are compared with the measured levels of the fundamental tone in table III.

It can be seen that good agreement is obtained for the QF-3 fan, on which the distortion measurements were made, and for the nearly similar QF-1 fan. However, the agreement with fans A and B is not very good. One possible explanation of the discrepancy is that the distortion entering fans A and B may not be the same as that measured on QF-3. Another possible explanation is that the analysis does not take into account the back reaction of the rotor potential-flow field on the inlet flow distortion. This back reaction could cause the distortion velocity distribution to be deformed before it interacts with the rotor. As a result the rotor would sense an inlet flow distortion with a higher harmonic content, which would then produce a scattered pressure field with more higher order modes. Since these modes will not be cut off as readily when the Mach number drops, more sound will be radiated at lower Mach numbers. Because fans A and B are run at lower Mach numbers than QF-1 and QF-3, the inclusion of this effect might improve the agreement with the data from the former fans.

A third possible explanation is that the outlet guide vanes in fans A and B, which are closer to the rotor than they are in QF-1 and QF-3, are producing some kind of rotor-stator interaction noise which is not being cut off. Finally, it should be noted that much of the energy in the discrete tones may be the result of unsteady flow distortions which cannot be detected by a velocity traverse made with a slow-response instrument such as a pitot tube rake.

CONCLUDING REMARKS

A combined dipole-quadrupole model (which includes the cross coupling between the two mechanisms) for predicting inlet flow distortion noise has been developed. Numerical results were obtained, and a comparison with the fundamental blade passing frequency noise from subsonic fan stages tested at the Lewis Research Center was made.

Very good agreement was obtained with data from a 51-centimeter (20-in.) model fan (tested indoors) by effectively adjusting the level of the theory so that it goes through a single point. This adjustment was necessary since the absolute amplitude of the distortion (which enters the equation as a multiplicative factor) was unknown. Good agreement was also obtained with the level of the fundamental tones measured on full-scale

fans. In this case, no adjustment was necessary since the distortion was measured. It should therefore be possible to use this model to study the noise reduction potential of the various design parameters of the fan.

Lewis Research Center,
National Aeronautics and Space Administration,
Cleveland, Ohio, March 7, 1974,
501-04.

APPENDIX - SYMBOLS

AR	aspect ratio
$A_{q,s}$	Fourier coefficient of axial distortion velocity
a_q	Fourier coefficient of circumferential distortion profile
B	number of blades
$B_{q,s}$	Fourier coefficient of radial distortion velocity
b	blade height
$C_{q,s}$	Fourier coefficient of circumferential distortion velocity
$C^{(0)}_{p,q,n}(\vec{x})$	defined by eq. (51)
$C^{\pm}_{m,n}(\vec{x},\omega)$	defined by eq. (18)
$dC_L/d\alpha$	lift slope
c	rotor chord length
c_0	speed of sound
D	compressibility correction factor defined by eq. (32)
$D^{\pm}_{m,n}$	defined by eq. (16b)
d_s	Fourier coefficient of radial distortion profile
$E_{m,s}$	defined by eq. (39)
e_{ij}	viscous stress tensor
F^0_q	Fourier coefficient of $\tilde{f}_\sigma$
$F^0_{\sigma,q}$	Fourier coefficient of f^0_σ
f	dimensionless circumferential distortion profile
f_j	force per unit area acting on cascade
f^0_σ	force on individual blade in cascade
$\tilde{f}_\sigma$	force per unit projected area acting on cascade
G	Green's function
g	radial distortion profile
$H_{p,q,s}$	defined by eq. (43)

$H^{(0)}_{p,q,s}$ defined by eq. (42)

I ratio of maximum distortion velocity to mean axial velocity U

$\bar{I}_p$ axial component of the sound intensity in the p^{th} harmonic

$K_{p,q,s}$ defined by eq. (44)

k wave number, ω/c_0

$k_{m,n}(k)$ propagation constants, $\sqrt{k^2 - \beta^2 \kappa^2_{m,n}}$

L_q Fourier coefficient of l

l lift force per unit length of blade

M axial Mach number, U/c_0

M_r relative Mach number, U_r/c_0

M_t rotor tip Mach number, U_t/c_0

N positive integer, $1, 2, \ldots$

P_D dipole contribution to sound pressure spectrum

P_Q quadrupole contribution to sound pressure spectrum

$P(\omega)$ sound pressure spectrum

$\mathscr{P}_p$ total acoustic power radiated upstream in the p^{th} harmonic

p' pressure measure above ambient pressure

p'_p p^{th} harmonic of acoustic pressure fluctuation

p_0 ambient pressure

$Q^{\pm}_{m,n}$ defined by eq. (16a)

$\bar{R}$ mean radius

S_a, S_b vertical duct surface area

S_f rotor surface area (relative to fixed coordinator)

S^0_f rotor surface (relative to rotor-locked coordinates)

$S(\sigma_q)$ Sears function

T large time interval (taken equal to infinity at end of analysis)

$T^{\dagger}_{ij}$ Lighthill's stress tensor based on relative velocity

t time (associated with observation point)

U axial flow velocity

U_r relative velocity, $-\sqrt{U_t^2 + U^2}$

U_t cascade (rotor) velocity

u_i distortion velocity

V_i phase-locked rotor velocity field relative to rotor blades, $i = 1,2$

v_i total fluid velocity

$v_i^\dagger$ relative velocity, $v_i - \delta_{1i}U$

v_p p^{th} harmonic of acoustic velocity

w_i phase-locked rotor velocity field

$\vec{X}$ coordinates fixed to rotor

$\vec{x}$ coordinates of observation point

$\vec{y}$ coordinates of source point

Z complex variable defined in terms of $\vec{X}$ coordinates by eq. (26)

z complex variable defined in terms of $\vec{\eta}$ coordinates by eq. (31)

$\alpha_i^\pm$ defined by eqs. (17)

β $\sqrt{1 - M^2}$

β_r $\sqrt{1 - M_r^2}$

β_t $\sqrt{1 - M_t^2}$

Γ_0 circulation about blade

γ stagger angle

Δ interblade spacing

Δ_0 defined by eq. (28)

δ circumferential distance, $B\Delta$

δ_{ij} Kronecker delta

$\delta(x)$ delta function

$\vec{\eta}$ rotor-locked coordinate system (eq. (12))

$\Theta_{p,q,s}$ defined in eq. (64)

θ work coefficient, $-\Delta w_2/U_t$

$\kappa_{m,n}$ eigenfunctions of wave operator

$\lambda_{s,q}$ defined by eq. (69)

$\nu(\tau)$ region of duct exterior to blades

ν_0 $\nu(\tau)$ at a fixed instant of time

ρ_0 background density

ρ' density fluctuation in acoustic field

σ', σ'' half-width of Gaussian/step profile

σ_q reduced frequency given by eq. (57)

$\tilde{\sigma}$ dimensionless radial hieght of flow distortion

τ time (emission)

$\Phi_{m,n}$ cross-duct eigenfunctions

ψ defined by eq. (65)

Ω shaft rotational frequency, $2\pi U_t/\delta$

ω frequency

Subscripts:

i,j,k integer 1,2,3

n integer 0,1,2,. . .

s integer 0,1,2,. . .

p,q integer 0,±1,±2,. . .

σ integer 1,2,. . .

Superscripts:

± upstream propagation/downstream propagation

† relative to coordinates moving with axial velocity U

$(\bar{\ })$ complex conjugate

REFERENCES

1. Mani, R.: Noise Due to Interaction of Inlet Turbulence with Isolated Stators and Rotors. Jour. Sound and Vib., vol. 17, no. 2, 1971, pp. 251-260.

2. Goldstein, M.; Rosenbaum, B.; and Albers, L.: Noise Generated by Inlet Turbulence. NASA TN D-7667, 1974.

3. Tyler, J. M.; and Sofrin, T. G.: Axial Flow Compressor Noise Studies. SAE Trans., vol. 70, 1962, pp. 309-332.

4. Sofrin, Thomas G.; and McCann, John C.: Pratt & Whitney Experience in Compressor-Noise Reduction. Paper presented at the 72nd meeting of the Acoustical Society of America (Los Angeles, Calif.), Nov. 1-5, 1966.

5. Goldstein, Arthur W.; Glaser, Frederick W.; and Coats, James W.: Effect of Casing Boundary-Layer Removal on Noise of a Turbofan Rotor. NASA TN D-6763, 1972.

6. Lowson, M. V.: Theoretical Analysis of Compressor Noise. Jour. Acoust. Soc. Am., vol. 47, no. 1 (part 2), 1970, pp. 371-385.

7. Povinelli, Frederick P.; Dittmar, James H.; and Woodward, Richard P.: Effects of Installation Caused Flow Distribution on Noise From a Fan Designed for Turbofan Engines. NASA TN D-7076, 1972.

8. Ffowcs Williams, J. E.; and Hawkings, D. L.: Theory Relating to the Noise of Rotating Machinery. Jour. Sound and Vib., vol. 10, no. 1, Jul 1969, pp. 10-21.

9. Morfey, C. L.: Tone Radiation From an Isolated Subsonic Rotor. Jour. Acoust. Soc. Am., vol. 49, no. 5 (part 2) 1971, pp. 1690-1692.

10. Goldstein, Marvin E.: Aeroacoustics. NASA SP-346, 1974, section 4.3.1.

11. Shapiro, Ascher H.: The Dynamics and Thermodynamics of Compressible Fluid Flow. Vol. II. Ronald Press Co., 1953.

12. Hayden, Richard E.: Noise from Interaction of Flow with Rigid Surfaces: A Review of Current Status of Prediction Techniques. NASA CR-2126, 1972.

13. McCormick, Barnes W., Jr.: Aerodynamics of V/STOL Flight. Academic Press, 1967.

14. Gelder, Thomas F.; and Soltis, Richard F.: Inlet Plenum Chamber Noise Measurement Comparison of 20-Inch Diameter Fan Rotors with Aspect Ratios 3.6 and 6.6. NASA TM X-2191, 1971.

TABLE I. - DESIGN PARAMETERS AND SUBSONIC OPERATING CONDITIONS FOR 51-CENTIMETER (20-IN.) MODEL FAN (ROTOR 1 - MODEL 1) AT 5 PERCENT OF SPAN FROM TIP

[Interblade spacing, Δ, 3.52 cm (1.385 in.); ratio of blade length to interblade spacing, b/Δ, 3.9; number of blades, B, 45; solidity, c/Δ, 1.3.]

Corrected fan speed, percent of design	Axial Mach number, M	Relative Mach number, M_r	Work coefficient, θ
80	0.525	0.973	0.129
	.463	.938	.307
	.382	.896	.322
70	0.480	0.864	0.0842
	.40	.818	.302
	.31	.771	.327
60	0.446	0.759	0.0508
	.340	.696	.294
	.268	.661	.331

TABLE II. - DESIGN AND OPERATING PARAMETERS FOR FULL-SCALE FAN STAGES AT 5 PERCENT OF SPAN FROM TIP (OPERATED WITH DESIGN NOZZLE)

Fan	Number of blades, B	Blade length, b		Interblade spacing, Δ		Solidity, c/Δ	Blade Mach number, M_t	Axial Mach number, M	Corrected fan speed, percent of design	Work coefficient, θ
		cm	in.	cm	in.					
QF-1	53	49	19.35	10.6	4.15	1.34	0.86	0.45	90	0.46
QF-3	53	49	19.35	10.6	4.15	1.34	.86	.45	90	.375
A	40	49.7	19.62	13.9	5.47	1.45	.815	.40	80	.425
B	26	49.7	19.62	21.5	8.45	1.30	.814	.40	80	.425

TABLE III. - COMPARISON OF THEORY WITH FULL-SCALE FAN STAGES (WITH OPERATING CONDITIONS OF TABLE II)

Fan	Experimental	Theory
	Power radiated in fundamental tone, dB	
QF-1	147	147
QF-3	146	145
A	147	142
B	149	141

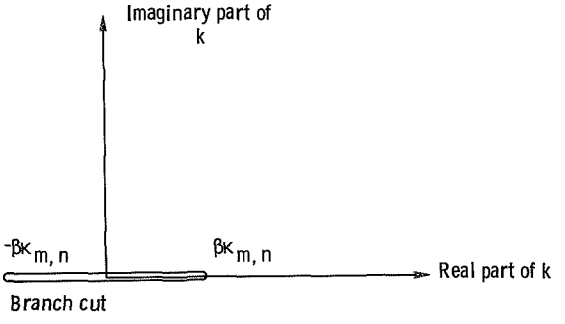

Figure 1. - Branch cut for $\sqrt{k^2 - \beta^2\kappa_{m,n}^2}$.

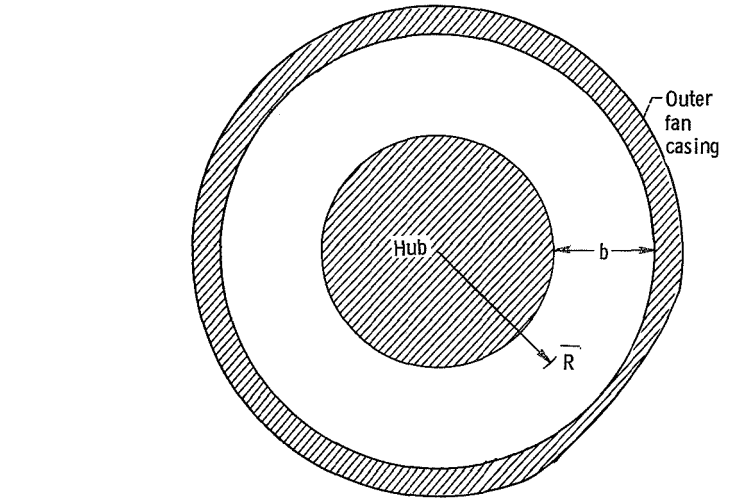

(a) Annular duct.

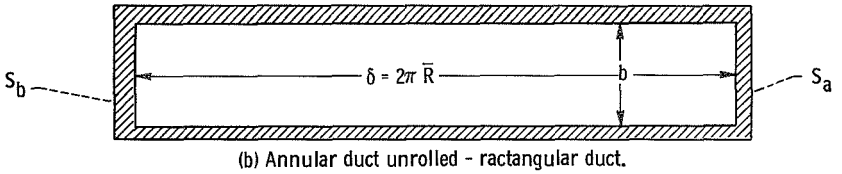

(b) Annular duct unrolled - ractangular duct.

Figure 2. - Duct cross section.

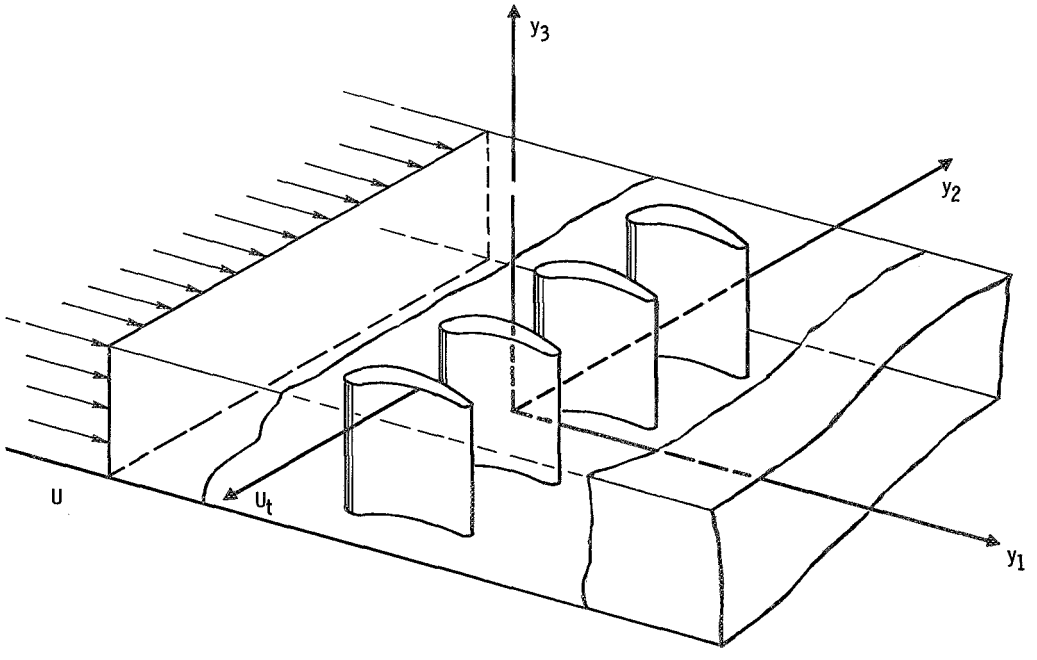

Figure 3. - Configuration of fan in rectangular geometry.

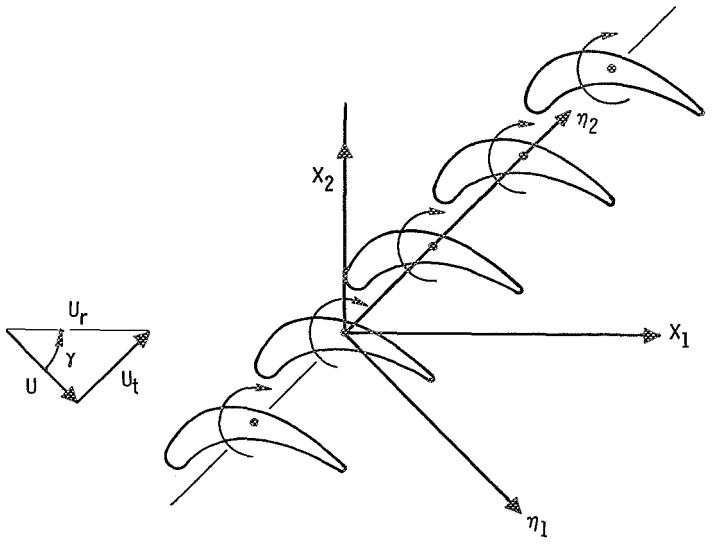

Figure 4. - Blade-oriented coordinate system.

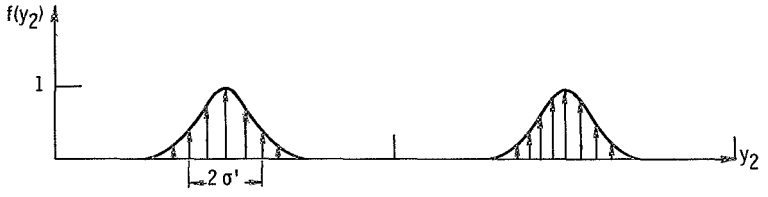

(a) Double-Gaussian-distortion velocity profile.

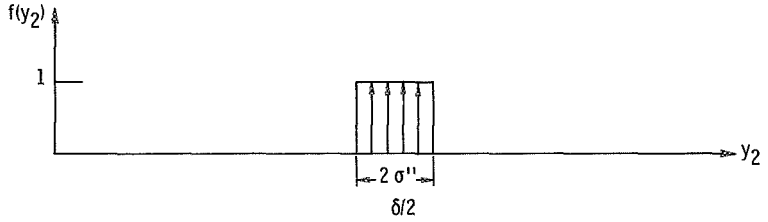

(b) Rectangular-distortion velocity profile.

Figure 5. - Radial variation of inlet flow distortion.

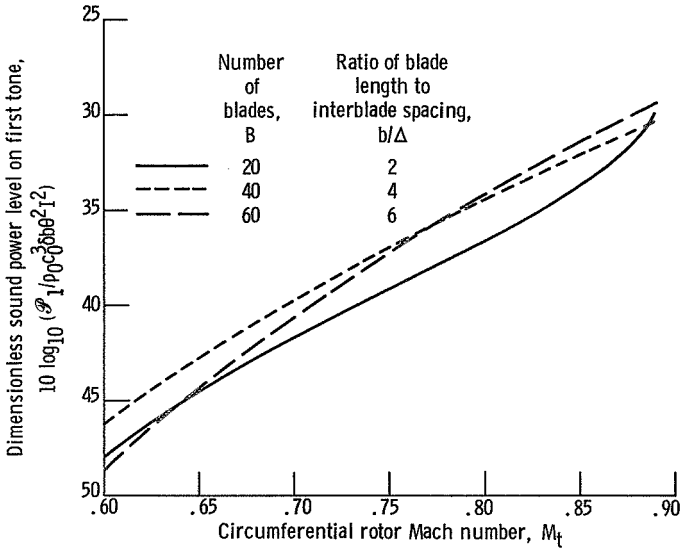

Figure 6. - Effect of blade number on power in fundamental tone. Half Half-width of Gaussian profile, σ', 0.1; dimensionless width of step profile, $\tilde{\sigma}$, 0.2; axial Mach number, $M = 1/2\, M_t$; solidity, c/Δ, 1.3; work coefficient, θ, 0.4.

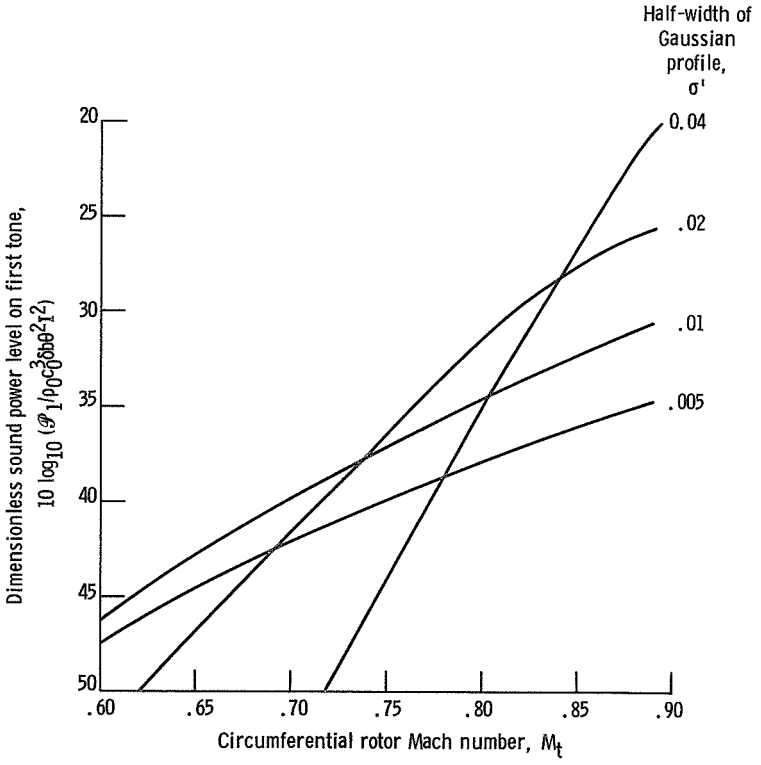

Figure 7. - Effect of distortion size on tone power level. Dimensionless width of step profile, $\tilde{\sigma}$, 0.2; Mach number, $M = 1/2\, M_t$; solidity, c/Δ, 1.3; number of blades, B, 40; work coefficient, θ, 0.4.

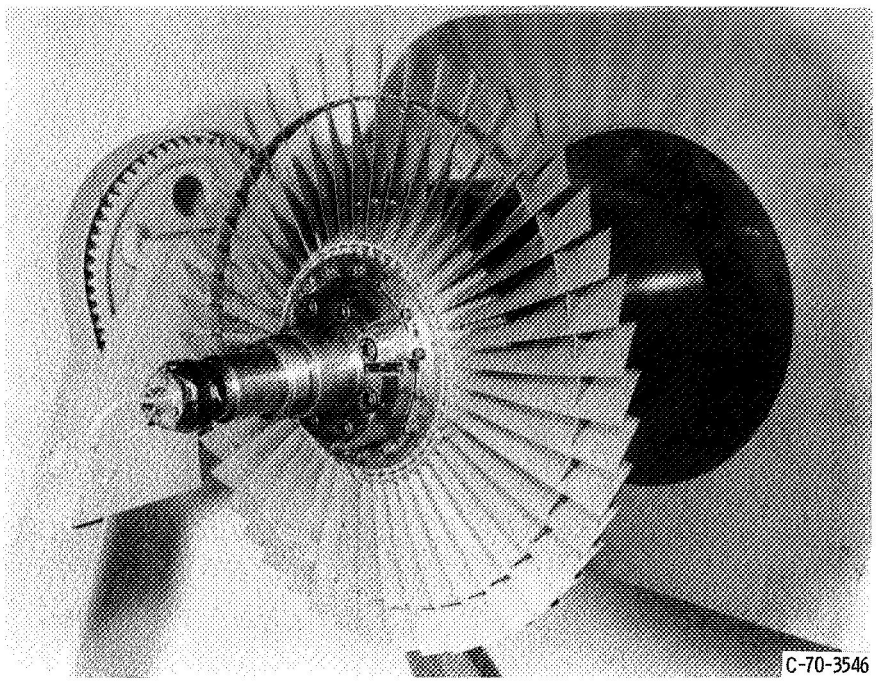

Figure 8. - Front-quarter view of rotor 1 - model 1.

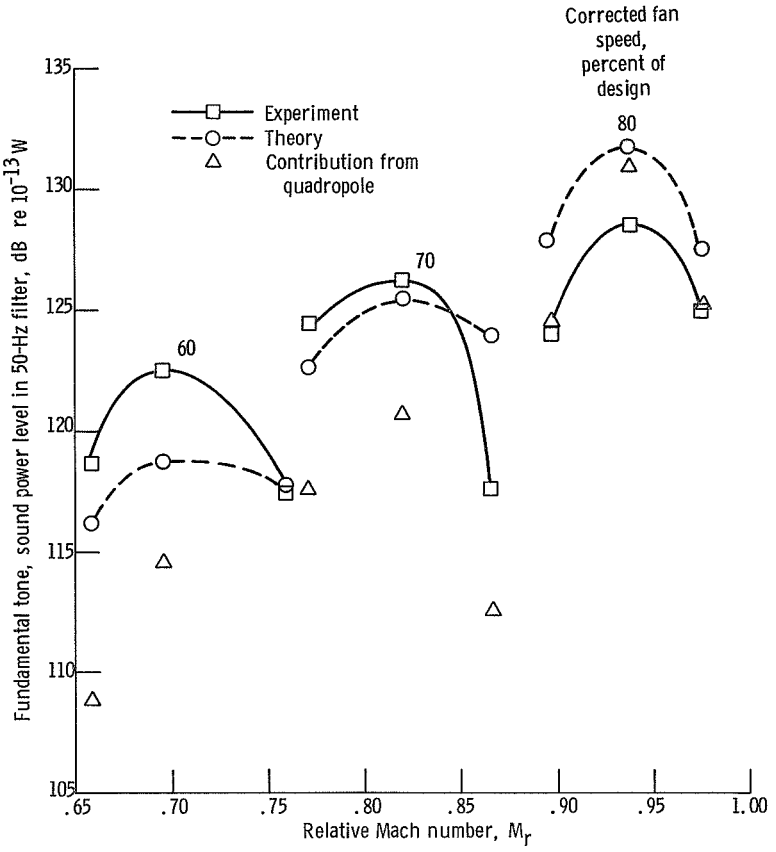

Figure 9. - Comparison of radiated sound power with 51-centimeter (20-in.) model fan (rotor 1 - model 1). Width of Gaussian profile, $2\sigma'$, 0.02; ratio of maximum distortion velocity to mean axial velocity, I, 0.015.

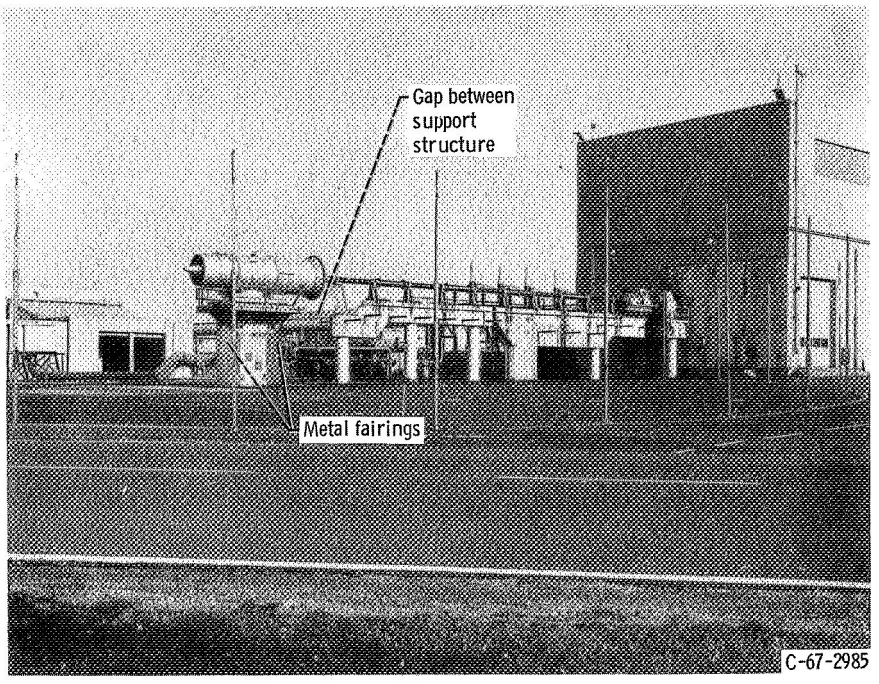

Figure 10. - Full-scale fan test installation.

NATIONAL AERONAUTICS AND SPACE ADMINISTRATION
WASHINGTON, D.C. 20546

OFFICIAL BUSINESS
PENALTY FOR PRIVATE USE $300

SPECIAL FOURTH-CLASS RATE BOOK

POSTAGE AND FEES PAID
NATIONAL AERONAUTICS AND SPACE ADMINISTRATION
451

U.S.MAIL

POSTMASTER: If Undeliverable (Section 158 Postal Manual) Do Not Return

"The aeronautical and space activities of the United States shall be conducted so as to contribute . . . to the expansion of human knowledge of phenomena in the atmosphere and space. The Administration shall provide for the widest practicable and appropriate dissemination of information concerning its activities and the results thereof."

—NATIONAL AERONAUTICS AND SPACE ACT OF 1958

NASA SCIENTIFIC AND TECHNICAL PUBLICATIONS

TECHNICAL REPORTS: Scientific and technical information considered important, complete, and a lasting contribution to existing knowledge.

TECHNICAL NOTES: Information less broad in scope but nevertheless of importance as a contribution to existing knowledge.

TECHNICAL MEMORANDUMS: Information receiving limited distribution because of preliminary data, security classification, or other reasons. Also includes conference proceedings with either limited or unlimited distribution.

CONTRACTOR REPORTS: Scientific and technical information generated under a NASA contract or grant and considered an important contribution to existing knowledge.

TECHNICAL TRANSLATIONS: Information published in a foreign language considered to merit NASA distribution in English.

SPECIAL PUBLICATIONS: Information derived from or of value to NASA activities. Publications include final reports of major projects, monographs, data compilations, handbooks, sourcebooks, and special bibliographies.

TECHNOLOGY UTILIZATION PUBLICATIONS: Information on technology used by NASA that may be of particular interest in commercial and other non-aerospace applications. Publications include Tech Briefs, Technology Utilization Reports and Technology Surveys.

Details on the availability of these publications may be obtained from:

SCIENTIFIC AND TECHNICAL INFORMATION OFFICE

NATIONAL AERONAUTICS AND SPACE ADMINISTRATION

Washington, D.C. 20546